Daytime Cirrus Cloud Top-of-the-Atmosphere Radiative Forcing Properties at a Midlatitude Site and Their Global Consequences

JAMES R. CAMPBELL

Naval Research Laboratory, Monterey, California

SIMONE LOLLI AND JASPER R. LEWIS

Joint Center for Earth Systems Technology, University of Maryland, Baltimore County, Baltimore, Maryland

YU GU

University of California, Los Angeles, Los Angeles, California

ELLSWORTH J. WELTON

NASA Goddard Space Flight Center, Greenbelt, Maryland

(Manuscript received 12 August 2015, in final form 14 April 2016)

ABSTRACT

One year of continuous ground-based lidar observations (2012) is analyzed for single-layer cirrus clouds at the NASA Micro Pulse Lidar Network site at the Goddard Space Flight Center to investigate top-of-the-atmosphere (TOA) annual net daytime radiative forcing properties. A slight positive net daytime forcing is estimated (i.e., warming): 0.07–0.67 W m^{-2} in sample-relative terms, which reduces to 0.03–0.27 W m^{-2} in absolute terms after normalizing to unity based on a 40% midlatitude occurrence frequency rate estimated from satellite data. Results are based on bookend solutions for lidar extinction-to-backscatter (20 and 30 sr) and corresponding retrievals of the 532-nm cloud extinction coefficient. Uncertainties due to cloud undersampling, attenuation effects, sample selection, and lidar multiple scattering are described. A net daytime cooling effect is found from the very thinnest clouds (cloud optical depth $\leq$ 0.01), which is attributed to relatively high solar zenith angles. A relationship involving positive/negative daytime cloud forcing is demonstrated as a function of solar zenith angle and cloud-top temperature. These properties, combined with the influence of varying surface albedos, are used to conceptualize how daytime cloud forcing likely varies with latitude and season, with cirrus clouds exerting less positive forcing and potentially net TOA cooling approaching the summer poles (not ice and snow covered) versus greater warming at the equator. The existence of such a gradient would lead cirrus to induce varying daytime TOA forcing annually and seasonally, making it a far greater challenge than presently believed to constrain the daytime and diurnal cirrus contributions to global radiation budgets.

1. Background

Cirrus clouds have long been recognized for their unique contribution to climate (Liou 1986). In particular, whereas all clouds warm the underlying atmosphere and surface at night [positive top-of-the-atmosphere (TOA) forcing], cirrus is the only genus that can readily warm or cool (negative TOA forcing; effectively all other clouds cool the daytime atmosphere) the daytime atmosphere and surface depending on the cirrus's varying physical characteristics [i.e., cloud height, temperature, effective particle size, surface thermal contrast, and ice water path–cloud optical depth; e.g., Stephens and Webster (1981)]. Conceptual models have long been established based on episodic regional measurements or modeling case studies depicting the offsetting relationship between cirrus cloud infrared absorption and reemission and solar albedo effects (e.g., Ackerman et al. 1988; Fu and Liou 1993; Jensen et al. 1994). They generally depict cirrus as daytime TOA warming agents, wherein clouds exhibiting

Corresponding author address: James R. Campbell, 7 Grace Hopper Ave., Stop 2, Monterey, CA 93943.
E-mail: james.campbell@nrlmry.navy.mil

DOI: 10.1175/JAMC-D-15-0217.1

an optical depth up to near 1.0 cause a positive net TOA forcing effect that exceeds the negative net forcing (cooling) by optically thicker clouds. Further, they imply that the most significant forcing comes from optically thicker clouds, wherein optically thin clouds contribute little to the overall forcing budget.

However these classical conceptual models, and thus the basis for our understanding of cirrus cloud forcing within the global cloud radiation budget, were built on regional or single-site datasets collected using long-antiquated remote sensing methodologies. Thus, they provide a fundamentally lesser understanding of the global variability in cirrus cloud physical properties and occurrence frequencies. With advanced ground and satellite-based observing systems established over recent years, progress is being made at refining these models and better isolating the net daytime forcing impact of cirrus clouds globally. In particular, we now recognize that cirrus clouds are the most common cloud genus observed (in terms of absolute frequencies) in the atmosphere (Stubenrauch et al. 2013 and references therein), with global occurrence frequencies ranging from 40% to 60% (Mace et al. 2009). Further, cirrus clouds skew heavily toward relatively low ice water content and low optical depth clouds (e.g., Sassen and Campbell 2001; Holz et al. 2008; Mace et al. 2009; Campbell et al. 2015).

The impact of this new and evolving understanding of cirrus has recently been highlighted by Berry and Mace (2014). They considered two years of integrated NASA A-Train Cloud Profiling Radar (CPR; Stephens et al. 2002) and Cloud–Aerosol Lidar with Orthogonal Polarization (CALIOP; Winker et al. 2010) cloud measurements over Southeast Asia, deriving a climatological model for tropical cirrus diurnal net TOA cloud forcing during the regional summer monsoon period. Specifically, they recognize that net cloud forcing functions, similar to those of the classic models outlined above, must be normalized by the relative frequencies of cloud occurrence. Accordingly, this shifts the relative burden of net cirrus cloud forcing toward more diffuse clouds, which are exponentially more prevalent, yielding a far more accurate net forcing budget that properly reconciles the climatic significance of optically thin clouds [optical depths < 0.3; Sassen and Cho (1992)] that is enhanced in the aggregate.

In this paper, net daytime TOA cirrus cloud forcing (CRF) is evaluated for data collected at a midlatitude site. Pairing a continuous 1-yr ground-based lidar-derived cirrus cloud observational dataset with a radiative transfer model, annual net daytime TOA cloud forcing characteristics are described. A slight positive annual net forcing (warming) is estimated overall. However, a net daytime cooling contribution is found from the very thinnest clouds, a discovery consistent with prior theory, and one that can be inferred from previous studies, although the process has yet to be specifically distinguished. Further, a distinct relationship involving the sign of the net daytime forcing is resolved as a function of the solar zenith angle and the cloud-top temperature (a proxy in this context for height). These properties in tandem, combined with consideration of varying surface albedos, imply that annual net daytime cirrus cloud forcing likely varies with latitude, which in turn raises questions as to how the sign and magnitude of the daytime cirrus forcing may vary seasonally with latitude and what the net daytime cirrus forcing contribution to the global radiation budget is overall. These processes are described, and the means for how they interrelate and impact net daytime TOA CRF solutions globally are hypothesized. The result is a relatively simple depiction of forcing characteristics for a distinct midlatitude site overall but, more importantly, a conceptual model for how variance in daytime cirrus forcing likely manifests meridionally over the global system.

2. Daytime cirrus TOA cloud radiative forcing calculations at Greenbelt, Maryland

a. 2012 MPLNET cirrus cloud subset at Greenbelt, Maryland

One year of continuous lidar-based cloud observations was collected in 2012 at the NASA Goddard Space Flight Center (GSFC) in Greenbelt, Maryland (38.99°N, 76.84°W; 0.050 km MSL) using a 532-nm NASA Micro Pulse Lidar Network instrument (MPLNET; http://mplnet.gsfc.nasa.gov/; Welton et al. 2001; Campbell et al. 2002). Cirrus clouds were retrieved from these data using signal-processing algorithms described in Campbell et al. (2008) and Lewis et al. (2015, manuscript submitted to *J. Atmos. Oceanic Technol.*, hereinafter LCHW) Specifically, however, genus discrimination is based on a thermal threshold that restricts the sample to clouds with a corresponding top-height temperature no warmer than −37°C. The justification for applying this restriction with respect to MPLNET profiling is outlined in Campbell et al. (2015), based on cirrus cloud climatological properties reported by Sassen and Campbell (2001) and given the single-channel elastic backscatter signal available currently from the instrument.

The daytime cirrus cloud subset analyzed here consists solely of single-layer scene clouds (i.e., only cirrus and no other clouds). This decision minimizes the influence of attenuation-limiting effects within the sample (i.e., in resolving cloud top and through multilayer structures). LCHW describe the use of 1-, 5-, and 20-min

sampling periods to resolve cirrus cloud presence in MPLNET products, wherein clouds are sought and distinguished at each resolution and regridded to a 1-min feature mask (1440 potential observations per day). Relatively high-resolution data sampling was thus applied for optimizing the instrument signal-to-noise ratio and retrieval performance at cirrus cloud altitudes during daylight hours [see Campbell et al. (2008) for an assessment of how MPL upper tropospheric cloud detection varies with temporal sampling resolution]. One-minute sampling was applied here at a nearly 3-to-1 rate more than the longer averages combined. A total of 21 107 single cirrus cloud layers were compiled and studied.

Daytime is designated in this study as being those hours when the incoming clear-sky net solar radiance exceeds the net outgoing energy. This condition limits apparent daylight hours versus those found with a more traditional definition based on solar zenith angle (SZA) relative to the horizon alone. Instead, this is an approximate threshold that segregates the diurnal cycle by contrasting periods where net TOA CRF can be both positive or negative (daytime) versus those where it can only be positive (nighttime; the impact of this decision within the analysis will be more clearly apparent in section 2d). Note that the true threshold separating such daily periods is always slightly lower with respect to the incoming solar radiance in the presence of cloud than that applied, depending on SZA, cloud physical properties, and thermal surface contrast. For practical purposes here, though, these differences are inconsequential. The distinction is critical, however, for isolating the sign and corresponding magnitude of the relative net daytime TOA CRF. The relative distribution of daytime to nighttime hours in this year-long analysis is approximately 40%–60%.

The 532-nm cloud extinction coefficient is the primary dependent lidar variable used to simulate cloud radiative properties (section 2b). MPLNET–single-channel elastic lidar solutions for the cirrus cloud extinction coefficient, however, are unconstrained (i.e., Fernald 1984), meaning that they cannot be solved directly. Therefore, the parameter is retrieved simultaneously here using both 20- and 30-sr values for the extinction-to-backscatter ratio (the so-called lidar ratio) (e.g., Garnier et al. 2015), to directly solve the lidar equation and resolve the ''bookend'' variance within the applied retrievals. [See Chew et al. (2011) for a similar instance in which such bookend lidar ratio solutions are applied to estimate the practical variance in MPLNET cirrus cloud extinction coefficient and optical depth analyses.] The two values are chosen broadly so as to account both for lidar ratio variability itself and for variance arising from subsequent system uncertainties introduced in the following discussion.

Multiple scattering is not considered in the solutions here for lidar extinction and cloud optical depth (COD). MPLNET instruments feature an unusually low field of view that generally suppresses the effects of multiple scattering. However, the presence of relatively large cirrus ice crystals corresponds with increasingly focused forward scattering of the laser along the forward-propagating plane, and thus the effect may become significant for portions of the cloud sample. MPLNET instruments have never been quantitatively evaluated for multiple scattering effects from clouds. Campbell et al. (2002) report an MPL field of view near 100 μrad. Estimates from Donovan and van Lammeren (2001) indicate that the impact for instruments featuring similar fields of view could be overestimates of total extinction and COD approaching 10%. However, the 100-μrad value has significantly decreased (by greater than 10%) in current MPLNET instruments, having integrated a more rugged and athermal telescope design that features a longer focal length than the original systems. It is therefore unclear how any such modeling estimates of multiple scattering practically relate to current versions of the technology.

Shown in Fig. 1 are probability distribution functions (PDFs) for frequencies of daytime cirrus cloud-top height altitude, depth, and top-height temperature from the 2012 GSFC sample, broken down into respective subsamples for COD solved using both 20 and 30 sr. Cloud tops vary in altitude between 6.0 and 16.0 km MSL for cloud-top temperatures ≤ -37°C and in cloud depth between 0.0 and 5.0 km. The relative frequency of cirrus observed during day versus night in the sample is almost exactly 40% versus 60%, implying there is no day–night data sampling bias present given those constraints introduced above. The sample is weighted decidedly, however, toward diffuse clouds. A total of 32% (24%) of the cloud samples correspond with subvisual cirrus [COD $\leq$ 0.03; cloud optical categories follow the classification rubric of Sassen and Cho (1992)] at 20 (30) sr. Accordingly, the higher extinction-to-backscatter value corresponds with greater COD, and the relative distribution shifts within each subsample. We find that 47% (42%) correspond with optically thin cirrus (0.03 $<$ COD $\leq$ 0.30) and 21% (34%) of the samples reflect relatively opaque clouds with COD $>$ 0.30 at 20 (30) sr.

Sampling bias at cirrus cloud altitudes is inherent to ground-based lidar observation as a result of signal attenuation from low-level liquid water clouds and through optically thick cirrus. Despite a reasonable and consistent set of sample constraints introduced above, for instance, attenuation effects can never be fully suppressed with respect to profiling above an initial cloud base. The result

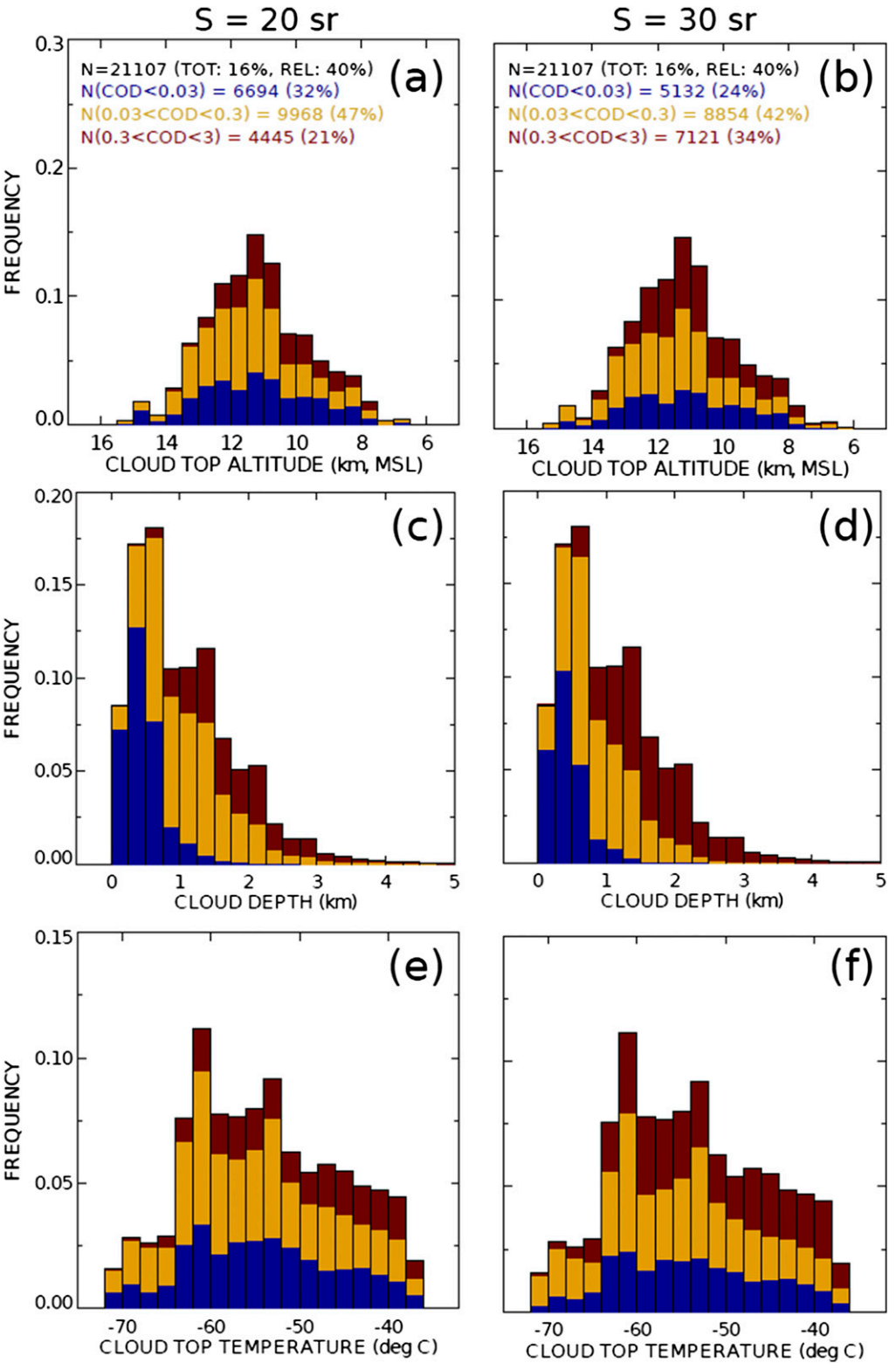

FIG. 1. Histograms of daytime cirrus cloud macrophysical properties at the MPLNET site in 2012 determined using (left) 20- and (right) 30-sr constraints for lidar extinction to backscatter *S*. Cloud properties are distinguished as functions of COD (≤0.03, blue; >0.03 and ≤0.30, yellow; >0.30, red) and include (a),(b) cloud-top height in 0.50-km intervals (MSL), (c),(d) cloud depth in 0.25-km intervals, and (e),(f) cloud-top temperature in 2°C intervals. Corresponding sample totals and relative percentages for each optical grouping and *S* value are included in (a) and (b).

is that some clouds are reported with a relatively low-biased cloud top, and thus a truncated extinction coefficient profile and low-biased COD estimate, and others are not identified at all within multilayer scenes. Sassen and Cho (1992) suggest that COD values between 3 and 5 reflect a practical upper limit for lidar cloud profiling because of increasing signal attenuation effects. Campbell et al. (2015) show that this value is likely closer to 2.4 in the current version-3 CALIOP datasets. COD estimates up to 3.0 are included in the 30-sr sample, as described above.

The lack of multilayer cirrus and liquid-water cloud scenes within the sample introduces an additional measure of sampling bias toward optically thinner clouds relative to attenuation effects alone. Such cases presumably tend toward higher COD. As a whole, the absolute daytime cirrus cloud frequency at GSFC within the sample is 16%, which is low by at least a factor of 2 relative to CALIOP observations in the midlatitudes (e.g., Mace et al. 2009). Of those clouds profiled, however, relative frequencies of thinner clouds within the sample are significantly higher than previous midlatitude estimates [80% (65%) of clouds with optical depths ≤ 0.30 at 20 (30) sr, respectively, versus ~50% found by Sassen and Campbell (2001)], thus very likely reflecting a disproportionate lack of relatively thicker clouds overall.

Thorsen et al. (2011) and Protat et al. (2014) describe sensitivities to cirrus cloud physical properties, relative frequencies of occurrence, and radiative characteristics derived from ground-based lidar and radar measurements, including MPLs operated by the Department of Energy, versus satellite-based profiling by CPR and CALIOP. Satellite sampling, and thus nadir-pointing profiling, overcomes many ground-based limitations, although it is by no means bias free either. CALIOP profiles the earth in a sun-synchronous orbital track, which inhibits daily diurnal cloud profiling at a single site, or potentially region, equally leading to unrepresentative sample datasets in their own right, particularly with respect to the focus of the current study. Reconciliation of corresponding ground-based and satellite studies, although relatively nascent, is a critical line of inquiry.

b. *Radiative transfer modeling system*

All cloudy and clear-sky contextual radiances considered here were solved using the Fu–Liou–Gu (FLG) radiative transfer model (Fu and Liou 1992, 1993; Gu et al. 2003, 2011). FLG is a combination of the delta-four-stream approximation for solar flux calculations (Liou et al. 1988) and a delta-two–four-stream approximation for IR flux calculations (Fu et al. 1997), which are divided into 6 and 12 bands, respectively. The delta-two–four-stream combination method is sufficiently economical for IR calculations (4 times faster than the delta-four-stream scheme, but only 50% more than the two-stream approach), and at the same time it produces acceptable accuracy under most atmospheric conditions. The *K*-distribution method is used to parameterize nongray gaseous absorption by CH_4, O_3, CO_2, and H_2O.

Cirrus cloud single-scattering properties in FLG are parameterized in terms of their ice water content and mean effective ice crystal diameter based on Liou et al. (2008; their section 3), repeated in Gu et al. [(2011); Eqs. (1)–(3)], with corresponding numerical coefficients determined from the scattering and absorption database compiled and reported by Yang et al. (2000) for the solar spectrum and Yang et al. (2005) for the infrared. The model assumes a mixed distribution of randomly oriented ice crystal shapes, consisting of 50% bullet rosettes, 30% columns, and 20% plates. Effective mean particle diameters and ice water contents are solved with empirical formulas built specially into the FLG model for this experiment [Eq. (9e) from Heymsfield et al. (2014)]. The effective mean particle diameter at each lidar range bin is solved based on the cloud temperature profile, derived for each case from version 5.9.1 of the Goddard Earth Observing System Model (GEOS-5; http://gmao.gsfc.nasa.gov/products) meteorological reanalysis dataset. The MPLNET-derived extinction coefficient is then paired with the effective mean particle diameter to solve for the ice water content at each corresponding bin.

Surface albedo values used in the model are monthly averaged broadband estimates based on Moderate Resolution Infrared Spectroradiometer (MODIS) measurements of integrated directional hemispherical reflectance near the GSFC site [black-sky albedo; Strahler et al. (1999)]. Values of broadband surface albedo range between 0.12 and 0.15 annually. An 11-μm land surface emissivity value of 0.97 is used, based on Jin and Liang (2006). A summary of all relevant model and input sample parameters relevant to the experimental design, and introduced to this point, is outlined in Table 1.

c. *Top-of-the-atmosphere daytime cirrus cloud forcing properties and uncertainties*

Figure 2a depicts the average daytime shortwave (SW), infrared (IR), and net daytime TOA CRF (defined as the difference in outgoing net TOA radiance in clear sky versus that for a given cloud, using a common thermodynamic profile) at both 20 and 30 sr as a function of COD in 0.03 resolution intervals between 0.00 and 3.00. These functions are expanded upon in scale in Fig. 2b, shown again at both 20 and 30 sr now as a function of

TABLE 1. A summary listing of primary experimental components and constraints used in this study.

Experimental component	Selection	Reference (if applicable)
Radiative transfer model	FLG delta-four stream system	Fu and Liou (1992, 1993); Gu et al. (2003)
Model meteorology	GEOS-5	Online (http://gmao.gsfc.nasa.gov/products)
Surface albedo	MODIS monthly averaged broadband values	Strahler et al. (1999)
Land surface thermal emissivity	0.97	Jin and Liang (2006)
Ice microphysical parameterization	—	Heymsfield et al. (2014)
Definition for daytime hours	Incoming clear-sky TOA solar radiation exceeds outgoing	—
Cirrus cloud dataset	MPLNET, version 3, cloud product	Campbell et al. (2008); LCHW (http://mplnet.gsfc.nasa.gov/)
Cirrus cloud thermal constraints	Cloud-top-height temperatures $\leq -37°C$	Campbell et al. (2015)

COD in 0.01 resolution intervals between 0.00 and 0.10. Since a consistent cloud sample is used for both the 20- and 30-sr solutions, and considering the analysis in Fig. 2a extends to COD = 3.00, this causes the maximum corresponding COD resolved at 20 sr to occur at only 0.73. Hence, this is why that function extends only to near that value, and why noise in that solution is apparent past about 0.70. The maximum net forcings are 3.78 and 5.71 $W m^{-2}$ at 20 and 30 sr, corresponding with 0.21 and 0.24 COD values, respectively. The primary crossover points between positive and negative net daytime TOA CRF apparent in Fig. 2a occur at 0.37 and 0.59 COD values, again at 20 and 30 sr, respectively.

Similar forcing profiles have been reported in previous regional studies (e.g., Fig. 13b in Ackerman et al. 1988; Fig. 3 in Jensen et al. 1994; Fig. 12b in Berry and Mace 2014). Given that each of those studies was set in the tropics and mostly over water however, and in the case of Jensen et al. (1994) and Berry and Mace (2014) reflect diurnal means where night and day are averaged together, differences seen between those profiles and the ones here are predominantly a reflection of being daytime profiles alone solved for midlatitude cirrus over land. How such differences are manifested in the results is discussed further in section 2d.

Shown in Fig. 3 are histograms of cirrus cloud relative frequency and net daytime TOA CRF normalized by the corresponding frequency at GSFC, again for both 20- and 30-sr solutions at 0.03 COD resolution between 0.00 and 3.00 (Figs. 3a,b) and at 0.01 COD resolution between 0.00 and 0.10 (Figs. 3c,d). These data are, again, qualitatively similar to those depicted in Berry and Mace (2014), although COD is the independent variable here as opposed to ice water path. Unlike the raw forcing relationships depicted in Fig. 2a however, which are the basis for the classical models described above, after normalizing by relative frequency, the maxima in positive net daytime TOA CRF (warming) correspond with COD below 0.10 in both solutions. Again from Fig. 1, 65% (80%) of the sample [30 (20) sr] corresponds with COD $\leq$ 0.30, which when normalized for in the net daytime TOA CRF relationships more appropriately resolves the relative warming component of those clouds in an apparent ''shift'' to lower COD relative to the unnormalized solutions. Primary crossover points between the positive and negative net daytime TOA CRF results occur near 0.35 (0.70) at 20 (30) sr, which is mostly unchanged from the unnormalized profiles in Fig. 2.

Integrated relative net daytime TOA CRF results solved from these data are 0.07 and 0.67 $W m^{-2}$ at 30 and 20 sr, respectively. For the 2012 annual GSFC cloud dataset examined here, the 16% absolute rate of occurrence for cirrus clouds observed again very likely reflects an undersampling of the total cirrus cloudiness at this site. Midlatitude cirrus cloud frequencies are nearer to 40%, based on Mace et al. (2009). Assuming that the distribution of relative cloud frequencies as a function of COD, as depicted in Fig. 3b, is reasonably representative despite undersampling, these results imply a slight positive cirrus net daytime TOA CRF (warming) annually at GSFC. That is, normalizing the forcing estimates to unity based on this satellite-based frequency estimate (i.e., normalizing them by 0.4), net daytime TOA CRF forcing estimated at this site in absolute terms then ranges between 0.03 and 0.27 $W m^{-2}$.

Of particular note is the identification of net daytime cooling at the very lowest COD cases (COD $\leq$ 0.01; Fig. 3d), as well as a secondary crossover point between positive and negative net daytime TOA CRF relative to Figs. 2a and 3a. Such a result has been hypothesized in FLG modeling sensitivity analyses (e.g., Min et al. 2010). Berry and Mace (2014) also report a very slight negative forcing component at their lowest ice water path values. Their cloud sample consists of all day–night ice-phase clouds above 10 km resolved with joint CPR–CALIOP measurements. Although slightly different than the experimental design considered here, the consistency with their finding is

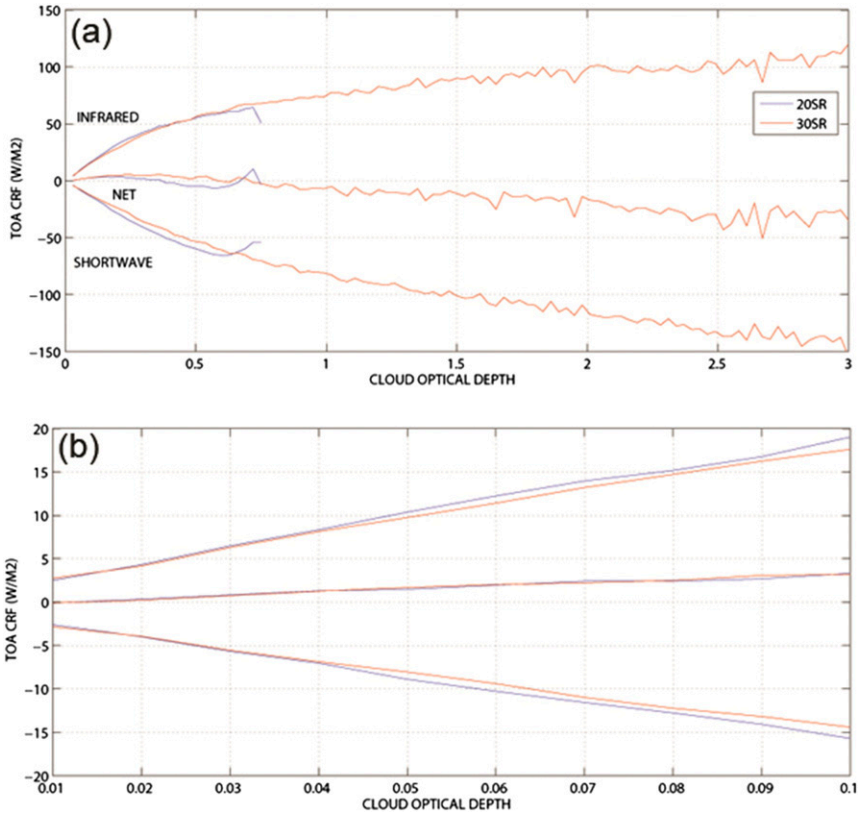

FIG. 2. For the 2012 daytime GSFC cirrus cloud subset, average TOA IR, SW, and net CRF for CODs (a) between 0.0 and 3.0 and (b) between 0.01 and 0.10, for the 20-sr (blue) and 30-sr (red) *S*-value solutions.

nevertheless compelling. The mechanics of this process relate to the influence on the net TOA CRF solution due to varying and increasing SZA, which is described in more detail in section 2d.

Based on Fig. 3b, and given the primary COD warming–cooling crossover points near 0.35 and 0.70 for 20 and 30 sr, respectively, undersampling due to attenuation and the lack of multilayer clouds is most likely affecting the sample of clouds disproportionately at COD values greater than both thresholds. Such clouds tend toward negative TOA CRF (cooling). Corresponding net daytime TOA CRF estimates are thus likely biased high as a result. However, this effect may be offset somewhat by the lack of relatively warm cirrus in the sample (cloud-top temperatures $> -37°C$), which Sassen and Campbell (2001) and Campbell et al. (2015) speculate are most likely sheared fallstreaks displaced from their parent cloud and thus are presumed likeliest to correspond with relatively low COD [positive net TOA CRF (warming); given their warmer nature, however, and thus lower thermal contrast with the surface, it is not absolutely clear that they would be significant warmers relative to colder portions of the sample]. If multiple scattering is significantly influencing the results, as well, the relative effect would be to bias COD low and thus net TOA CRF high, which would exacerbate the effects of undersampling at higher COD.

It is ultimately unclear exactly how each of these relative uncertainties is affecting the net solutions. Given the distinct disproportionality of optically thin clouds within the sample compared with previous studies, however, and combined with the uncertainty of multiple scattering effects, estimates of net daytime TOA CRF reported here are believed to be likelier to be biased high relative to the counterbalancing effects within the sample caused by disregarding warm cirrus. To be clear, though, the net daytime TOA CRF values reported here are strictly estimates given the constraints of the input data assembled, and presumably within the practical bounds of the two lidar ratios applied to render cloud extinction. Still, the results are unique, albeit in a qualified manner, reflecting a methodology designed to render the most practical estimate currently possible from autonomous ground-based lidar profiling.

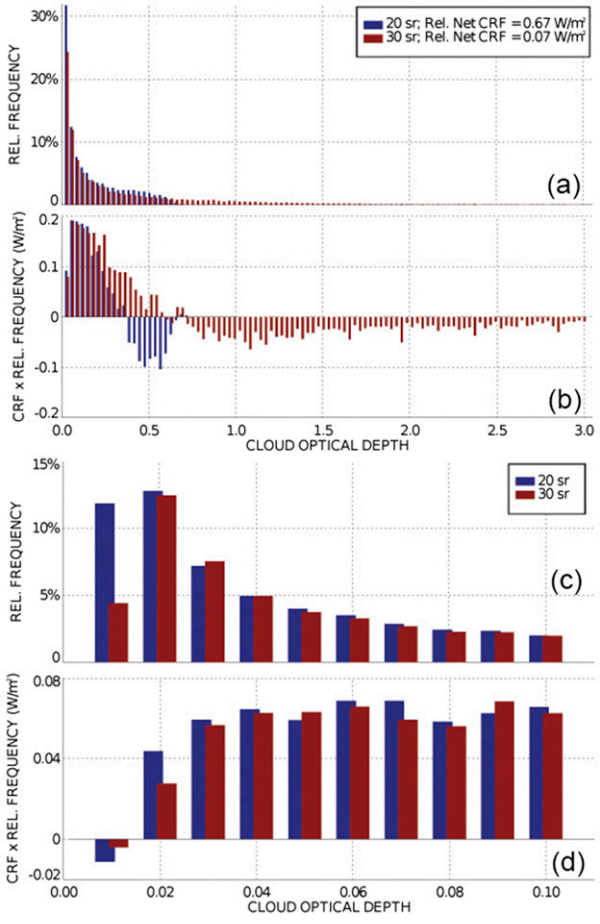

FIG. 3. For the 2012 daytime GSFC cirrus cloud subset, (a) relative frequency of cloud occurrence vs COD and (b) average net TOA CRF from Fig. 2a normalized by relative frequency in (a), both in 0.03 COD intervals between 0.0 and 3.0 for the 20-sr (blue) and 30-sr (red) *S*-value solutions. (c),(d) As in (a) and (b), but in 0.01 COD intervals between 0.0 and 0.1.

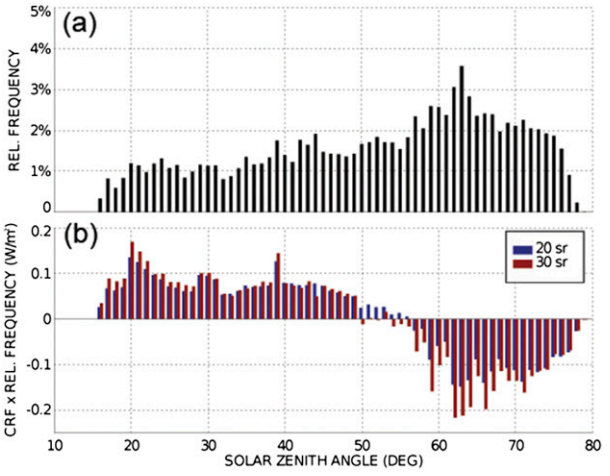

FIG. 4. For the 2012 daytime GSFC cirrus cloud subset, (a) relative frequency of cloud occurrence vs SZA in 1° intervals (see text for specific definition for daytime hours) and (b) corresponding average net TOA CRF (Fig. 2a) normalized by these frequencies, for the 20-sr (blue) and 30-sr (red) *S*-value solutions.

d. Daytime TOA forcing versus cloud-top heights/temperatures and its latitudinal dependence

Relative frequencies of daytime cirrus cloud occurrence as a function of SZA in 1° intervals and their corresponding normalized net TOA CRF are shown in Figs. 4a and 4b, respectively. A crossover point between net positive (warming) and negative (cooling) is found near 55° in both the 20- and 30-sr solutions. Cloud occurrence corresponds most frequently with relatively higher SZA and negative net forcing. Despite the slightly positive net integrated daytime TOA CRF estimated above, the normalized net TOA CRF per degree is generally greater at higher relative SZAs.

The basis for restricting daytime hours in this study to those for which incoming net TOA clear-sky solar radiation exceeds outgoing total energy is borne out in Fig. 4b. As SZA increases toward 80°, which proves the approximate effective annual SZA threshold found by applying the definition to these data, the mean net daytime TOA CRF gradually converges from negative (i.e., cooling) toward zero. It eventually becomes strongly positive (i.e., warming; not shown), under what are defined as nighttime conditions. As described above, as incoming solar radiation lessens with increasing solar angle, near the point where the total incoming energy equals that outgoing, the solution for net daytime TOA CRF can never turn negative (again, with slight caveats due to SZA, COD, and the thermodynamic profile, although the data shown in Fig. 4b verify that this offset is mostly negligible) and all clouds become TOA warming elements. Therefore, the approximated threshold is applied as the only practical means for isolating the potential fluctuation in the sign of net daytime cirrus cloud TOA CRF, which can only occur under relatively significant solar insolation during daytime hours. Critically, previous attempts to reconcile cirrus net TOA CRF properties have considered only the diurnal mean value (e.g., Fig. 4 in Fu et al. 2002), as opposed to isolating the specific attributes exhibited by cirrus under solar illumination.

The impact of increasing SZA on net daytime TOA CRF is to enhance cloud solar extinction relative to thermal effects. As SZA deviates from 0°, the propagation angle of incoming solar energy incident at cloud top changes while thermal emissions below and within the cloud remain effectively oriented in the zenith–nadir plane. Therefore, as SZA increases, the effective solar COD increases by extending the propagation length within a cloud, increasing the relative scattering [i.e., Beer's law; Sun et al. (2011) infer a similar effect] and

the net solar forcing component relative to an effectively static thermal one. As seen in Fig. 2b, however, at relatively low COD this change in effective solar COD can influence the sign of the net solution relating solar and infrared forcing. Ackerman et al. (1988) and Fu and Liou (1993) imply that that the relationship is otherwise always positive, given a reasonably low SZA and for a common range of effective particle sizes. At relatively high SZAs, however, as relative solar COD increases, the sensitivity of the relationship is such that the sign can reverse. Net daytime TOA CRF near COD = 0.01 depicted in Fig. 2b reflects such a reversal in the aggregate, which is the point of enlarging the scale in that figure relative to Fig. 2a and likely an important consideration as to why previous researchers, Min et al. (2010) aside (although one has to look very carefully at their result to resolve it), have not recognized this process.

It is critical, though, to recognize that SZA frequency distributions vary with latitude and season, as compared with that solved annually here for this single midlatitude site. Therefore, the distinct relationship between the sign of the net daytime TOA cirrus cloud forcing and SZA in this analysis implies that a latitudinal variation in net daytime TOA CRF exists globally. Min et al. (2010) conceptualize how the combination of fluctuating regional surface albedo and variation in mean macrophysical cirrus cloud properties found with latitude could influence the relative distribution of positive and negative daytime cirrus TOA CRF results relative to SZA. Sassen and Campbell (2001) broadly speculate on such variability being plausible. The results here are the first evidence, however, of how such variance is reflected in actual observations.

The frequency of cloud occurrence for relatively high SZA (>55°) increases moving poleward, which will presumably lead to gradually greater relative net daytime cloud cooling. Further, lowering the mean cloud heights toward the poles and less thermal contrast between the clouds and surface would suppress the positive relative infrared forcing term (Corti and Peter 2009), as would the impact of offsetting cooling by the very lowest COD layers that would also increase in significance given the greater frequency of higher SZA cases. The scenario would then reverse, moving from the midlatitudes toward the equator, leading to greater relative positive daytime forcing (warming) there. Similarly, the primary crossover COD threshold at higher values, above which negative net TOA solar forcing exceeds the positive infrared component and clouds become net daytime cooling agents, will be suppressed (enhanced) by a higher (lower) mean effective SZA for a given site, which will also significantly influence net daytime TOA CRF values.

In winter, high surface albedos over ice and snow and fewer daylight hours available will offset many of these factors approaching the seasonal pole (higher albedos induce a greater positive relative solar daytime TOA CRF component and are thus consistent with greater net positive daytime TOA CRF overall; Min et al. 2010). During summer, though, as ice and snow-covered regions retreat, and considering the greater number of daytime hours available relative to polar night combined with endemically higher SZA, a significant meridional gradient in net daytime cirrus cloud forcing between warming at the equator and likely cooling near the corresponding pole likely occurs. The slightly positive forcing value solved at this midlatitude site would thus represent a location nearing the approximate midpoint along this hypothetical gradient. Further, given the increase in relative surface albedo over oceans at low SZA (Jin et al. 2004), warming is likely enhanced even further near the equator, which exacerbates this scenario. Most fascinating about this potential feedback mechanism, though, is its apparent paradoxical nature. If present, positive (negative) daytime cirrus TOA CRF would reinforce warming (cooling) near the equator (summer pole). This, in turn, would act to strengthen the meridional temperature gradients, and thus baroclinicity, most prominently in the summer hemisphere when ice coverage and nighttime hours are at seasonal minimums.

Variability in ice microphysical properties with latitude and season will prove a unique consideration when evaluating the merits of this hypothesis in future work. For instance, Liou et al. (2008) describe field measurements that imply distinct latitudinal variability in effective particle diameter as a function of ice water path. FLG, in fact, features settings that allow the user to vary this relationship within the model. The Heymsfield et al. (2014) parameterization relating lidar extinction with ice water content, effective particle diameter, and cloud temperature built into FLG for this study, however, is based on the premise that many field measurements of ice microphysical properties suffer from sampling bias, induced by the shattering of crystals on the inlets of the instruments designed to measure them. Instead, their parameterization is latitude neutral, thus reconciling all apparent hemispheric variability between those three dependent parameters. Endemic differences in single-scattering properties induced by meridional ice microphysical variability would influence how net daytime TOA CRF is distributed, however, and therefore must be considered. Still, with respect to Liou et al. (2008), they suggest that the solar cloud albedo near the poles at a relative maximum compared with the midlatitudes and tropical clouds, which, if true [notwithstanding the

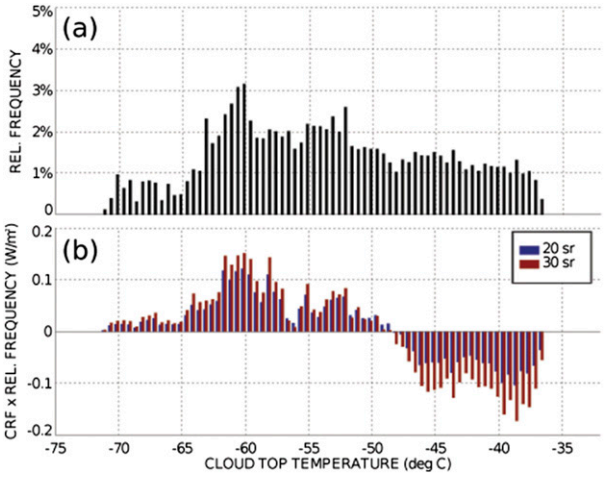

FIG. 5. For the 2012 daytime GSFC cirrus cloud subset, (a) relative frequency of cloud occurrence vs cloud-top temperature in 0.5°C intervals ≤−37°C (see text for justification) and (b) corresponding average net TOA CRF (Fig. 2a) normalized by these frequencies, for the 20-sr (blue) and 30-sr (red) *S*-value solutions.

concerns outlined in Heymsfield et al. (2014)], would likely exacerbate the proposed gradient further (i.e., greater cooling).

The remaining consideration in this paradigm, then, is the mean distribution of cirrus cloud heights and their sensitivity to net daytime TOA CRF. Shown in Fig. 5, similar to Fig. 4, is the frequency of cloud-top heights in 2012 at GSFC as a function of temperature (°C) in ½° intervals and the corresponding frequency-normalized net daytime TOA CRF. Infrared CRF is a direct function of the difference in surface temperature and blackbody emissions temperature of the overlying cloud (e.g., Corti and Peter 2009). Therefore, the coldest clouds correspond with the greatest thermal forcing and a positive (warming) daytime TOA CRF overall. A singular crossover point between net warming and cooling occurs near −48°C. Whereas the relative frequency of cloud occurrence increases for colder temperatures, a resulting distribution that is broadly consistent with that of midlatitude cirrus clouds reported in Campbell et al. (2015) from CALIOP observations, cloud cooling is still relatively significant for the warmer cases. Moving poleward, mean cloud heights decrease as does the thermal contrast between the clouds and the surface. During summer months when the snow and ice ground cover again retreats, lowering relative surface albedos, this distribution will very likely skew toward greater negative net daytime TOA CRF. The opposite would then be expected moving toward the equator, with greater warming and positive net daytime TOA CRF apparent, although endemically smaller ice crystals associated with colder convection (e.g., Heymsfield et al. 2014) will in fact lower the relative infrared warming term. Future work with the MPLNET datasets in tropical locations, such as Singapore (e.g., Chew et al. 2011), will shed light on how the relationship bears out in practice near the equator.

3. Conclusions

Perhaps the most important contribution made by autonomous lidar monitoring projects, like MPLNET and CALIOP, to furthering our understanding of global cloud physical processes over the last decade is in the recognition that optically thin cirrus clouds [cloud optical depths < 0.3; Sassen and Cho (1992)] are the most common cloud type in the earth–atmosphere system (e.g., Mace et al. 2009; Stubenrauch et al. 2013). Cirrus clouds represent the last tropospheric barrier to water vapor escaping the hydrologic cycle, and can thus be found over all global regions during all seasons. Their significance to climate and radiative balance, despite episodic net top-of-the-atmosphere cloud radiative forcing values generally on the order of only 1–10 $W m^{-2}$ as compared with liquid water clouds that exert TOA CRF on the order of 100 $W m^{-2}$, is grounded in the long-term aggregate, enhanced by their relatively high occurrence rate and global extent. This fundamental relationship has been recently illustrated by Berry and Mace (2014). With increasingly long-term observations of cirrus clouds globally made possible by continuous ground and satellite-based lidar monitoring, the goal of accurately constraining seasonal and annual cirrus net daytime and diurnal TOA CRF is increasingly achievable, which will yield a better understanding of the role cirrus clouds play in cloud radiative budgets overall.

In this paper, one year's worth (2012) of continuously running NASA MPLNET 532-nm ground-based lidar observations of single-layer cirrus clouds collected at the NASA Goddard Space Flight Center are investigated for TOA annual net daytime cloud radiative forcing properties. A slight positive annual net daytime TOA CRF is estimated, varying between approximately 0.07 and 0.67 $W m^{-2}$ in relative terms and 0.03 and 0.27 $W m^{-2}$ in absolute terms. The latter result is reached after normalizing the relative estimate based on a satellite-approximated 40% midlatitude cirrus cloud occurrence frequency. The methodology features bookend solutions for cloud extinction estimated from the elastic lidar observations available (20- and 30-sr settings for the so-called lidar ratio) in order to initialize the Fu–Liou–Gu radiative transfer model. Estimate uncertainties arise from the undersampling of cases with relatively high cloud optical depth, a lack of multilayer cloud scenes, sample limits for

cirrus to clouds with top-height temperatures $\leq -37°C$, and the unresolved impact of laser multiple scattering. Therefore, these values are strictly estimates of net daytime cirrus TOA CRF at this site, with the bounds of the lidar ratio settings chosen broadly to approximate any system variance encountered. This work represents the first known attempt to specifically distinguish daytime cirrus net TOA CRF, applying a unique definition for daytime that isolates the potential fluctuation in net daytime TOA CRF sign that can only occur when clouds are illuminated by solar radiance above a threshold roughly equal to the clear-sky outgoing energy.

Specific features of the annual daytime TOA CRF relationship are highlighted in the analysis. From the very thinnest clouds (COD $\leq$ 0.01), a net negative daytime TOA CRF (cooling) is identified. Given that relative cloud frequencies are very high in the sample at these extremely low optical depths, there is some consequential offsetting of bulk warming occurring from optically thin clouds that impacts the annual net total. This process is attributed to relatively high solar zenith angles, and increasing effective solar optical depths relative to thermal cloud absorption and emissions that remain effectively oriented in the zenith–nadir planes. For the relatively low solar and infrared TOA CRF values occurring within these clouds at such low COD, the effect is enough to turn the net solution negative in the aggregate.

A distinct relationship involving net positive/negative daytime TOA CRF is also demonstrated as a function of solar zenith angle and cloud-top temperature (a proxy in this context for height). Combined with the influence of surface albedo on TOA CRF, the results at GSFC are used to conceptualize how cloud forcing likely varies with latitude and season, with cirrus clouds hypothesized as being net TOA daytime warming elements at the equator, consistent with existing models, to gradually exerting less positive forcing, and likely a net TOA daytime cooling, approaching the poles. Consequentially, the slightly positive value estimated at this midlatitude site is believed to represent a point nearing the middle of such a hypothetical meridional gradient. The gradient effect is likely strongest in the summer hemisphere, from lesser relative surface albedos, and more daylight hours and high SZAs nearing the poles combined with low SZAs near the equator that enhances surface albedo over open waters and increases TOA warming. It is unclear to what degree the meridional variability in ice microphysical properties may influence this process.

Such a gradient, if proven true, would reflect the discovery of a fundamental atmospheric feedback mechanism that acts to increase hemispheric thermal gradients and baroclinicity. In the summer hemisphere, when such gradients are seasonally relaxed compared with winter, this progressive forcing mechanism would represent a significant new process to resolve within global climate simulations. Most prominently, however, is the binding characteristic that cirrus clouds are the only cloud genus that can yield a positive net daytime TOA CRF in the first place. A fluctuating meridional forcing gradient, as such, would be a wholly unique atmospheric process alone within that context. This potential finding thus represents a fundamentally new way of considering how cirrus clouds impact TOA energy budgets overall.

This work further reinforces how classical conceptual models for cirrus cloud TOA CRF estimates are based on an antiquated understanding of the physical properties and global distribution of cirrus clouds, which overemphasizes the impact of optically denser clouds. Evidence has long mounted, raising question as to how these models were manifested globally. For instance, Stephens et al. (1990) identify a lower threshold in effective cloud particle size whereby the relationship reverses, and cloud solar reflection exceeds infrared warming at much lower optical depths than believed common. Khvorostyanov and Sassen (2002) describe three modeling scenarios for midlatitude cirrus cloud occurrence, finding a net daytime cloud cooling in all three cases. Barja and Antuna (2011) report similar results in a limited lidar cloud sample over Cuba. Here, and on the heels of the work of Berry and Mace (2014) in Southeast Asia, the impact of relative cirrus cloud frequencies that skew heavily to optically thin clouds is more appropriately considered. This analysis thus further develops a foundational basis for extrapolating these results, and the processes resolved, to the global scale, with demonstrable hypotheses on how global daytime net cirrus TOA CRF varies with latitude and season and what impacts daytime cirrus have to the climate radiation budget as a whole.

One final point comes about from the sustained importance of ground-based profiling of cirrus clouds, in spite of the ever-burgeoning satellite era anchored currently by CALIOP and in anticipation of additional future missions. Ground-based observations continue providing critical satellite ground truth, albeit with caveats. Most important, though, they continue providing diurnal observations. This study demonstrates specifically how SZA influences solutions for cirrus net daytime TOA CRF, for instance. Although Min et al. (2010) attempt to circumvent this aspect of the sun-synchronous CALIOP dataset in a similar study of cirrus cloud radiative properties, the role for continuous ground-based remote sensing remains clearly defined within this context. As Thorsen et al. (2011) and Protat et al. (2014)

have demonstrated, whereas ground-based lidar profiling is subject to observational bias (due to attenuation limits caused mostly by low-level liquid water clouds, but also by thicker cirrus themselves), there remains significant information content in long-term ground-based datasets for providing regional context fundamental to reconciling satellite measurements. With hopes of quantifying the global, regional, annual, seasonal, and even diurnal distribution of cirrus net TOA CRF, looking forward to a study similar to this based on CALIOP datasets, the synergy between ground and satellite observation should be leveraged to best constrain uncertainties and render the most accurate result currently possible.

Acknowledgments. The NASA Micro Pulse Lidar Network (MPLNET) is supported by the NASA Radiation Sciences Program (H. Maring). JRC acknowledges the support of NASA Interagency Agreement NNG15JA17P on behalf of MPLNET.

REFERENCES

Ackerman, T. P., K.-N. Liou, F. P. J. Valero, and L. Pfister, 1988: Heating rates in tropical anvils. *J. Atmos. Sci.*, **45**, 1606–1623, doi:10.1175/1520-0469(1988)045<1606:HRITA>2.0.CO;2.

Barja, B., and J. C. Antuna, 2011: The effect of optically thin cirrus clouds on solar radiation in Camagüey, Cuba. *Atmos. Chem. Phys.*, **11**, 8625–8634, doi:10.5194/acp-11-8625-2011.

Berry, E., and G. G. Mace, 2014: Cloud properties and radiative effects of the Asian summer monsoon derived from A-Train data. *J. Geophys. Res.*, **119**, 9492–9508, doi:10.1002/2014JD021458.

Campbell, J. R., D. L. Hlavka, E. J. Welton, C. J. Flynn, D. D. Turner, J. D. Spinhirne, V. S. Scott, and I. H. Hwang, 2002: Full-time, eye-safe cloud and aerosol lidar observation at Atmosphere Radiation Measurement program sites: Instrument and data processing. *J. Atmos. Oceanic Technol.*, **19**, 431–442, doi:10.1175/1520-0426(2002)019<0431:FTESCA>2.0.CO;2.

——, K. Sassen, and E. J. Welton, 2008: Elevated cloud and aerosol layer retrievals from micropulse lidar signal profiles. *J. Atmos. Oceanic Technol.*, **25**, 685–700, doi:10.1175/2007JTECHA1034.1.

——, M. A. Vaughan, M. Oo, R. E. Holz, J. R. Lewis, and E. J. Welton, 2015: Distinguishing cirrus cloud presence in autonomous lidar measurements. *Atmos. Meas. Tech.*, **8**, 435–449, doi:10.5194/amt-8-435-2015.

Chew, B. N., J. R. Campbell, J. S. Reid, D. M. Giles, E. J. Welton, S. V. Salinas, and S. C. Liew, 2011: Tropical cirrus cloud contamination in sun photometer data. *Atmos. Environ.*, **45**, 6724–6731, doi:10.1016/j.atmosenv.2011.08.017.

Corti, T., and T. Peter, 2009: A simple model for cloud radiative forcing. *Atmos. Chem. Phys.*, **9**, 5751–5758, doi:10.5194/acp-9-5751-2009.

Donovan, D. P., and A. C. A. P. van Lammeren, 2001: Cloud effective particle size and water content profile retrievals using combined lidar and radar observations 1. Theory and examples. *J. Geophys. Res.*, **106**, 27 425–27 448, doi:10.1029/2001JD900243.

Fernald, F. G., 1984: Analysis of atmospheric lidar observations: Some comments. *Appl. Opt.*, **23**, 652–653, doi:10.1364/AO.23.000652.

Fu, Q., and K. N. Liou, 1992: On the correlated *k*-distribution method for radiative transfer in nonhomogeneous atmospheres. *J. Atmos. Sci.*, **49**, 2139–2156, doi:10.1175/1520-0469(1992)049<2139:OTCDMF>2.0.CO;2.

——, and ——, 1993: Parameterization of the radiative properties of cirrus clouds. *J. Atmos. Sci.*, **50**, 2008–2025, doi:10.1175/1520-0469(1993)050<2008:POTRPO>2.0.CO;2.

——, ——, M. Cribb, T. P. Charlock, and A. Grossman, 1997: Multiple scattering parameterization in thermal infrared radiative transfer. *J. Atmos. Sci.*, **54**, 2799–2812, doi:10.1175/1520-0469(1997)054<2799:MSPITI>2.0.CO;2.

——, M. Baker, and D. L. Hartman, 2002: Tropical cirrus and water vapor: An effective Earth infrared iris feedback? *Atmos. Chem. Phys.*, **2**, 31–37, doi:10.5194/acp-2-31-2002.

Garnier, A., J. Pelon, M. A. Vaughan, D. M. Winker, C. R. Trepte, and P. Dubuisson, 2015: Lidar multiple scattering factors inferred from *CALIPSO* lidar and IIR retrievals of semi-transparent cirrus cloud optical depths over oceans. *Atmos. Meas. Tech.*, **8**, 2759–2774, doi:10.5194/amt-8-2759-2015.

Gu, Y., J. Farrara, K. N. Liou, and C. R. Mechoso, 2003: Parameterization of cloud–radiation processes in the UCLA general circulation model. *J. Climate*, **16**, 3357–3370, doi:10.1175/1520-0442(2003)016<3357:POCPIT>2.0.CO;2.

——, K. N. Liou, S. C. Ou, and R. Fovell, 2011: Cirrus cloud simulations using WRF with improved radiation parameterization and increased vertical resolution. *J. Geophys. Res.*, **116**, D06119, doi:10.1029/2010JD014574.

Heymsfield, A., D. Winker, M. Avery, M. Vaughan, G. Diskin, M. Deng, V. Mitev, and R. Matthey, 2014: Relationships between ice water content and volume extinction coefficient from in situ observations for temperatures from 0° to −86°C: Implications for spaceborne lidar retrievals. *J. Appl. Meteor. Climatol.*, **53**, 479–505, doi:10.1175/JAMC-D-13-087.1.

Holz, R. E., S. A. Ackerman, F. W. Nagle, R. Frey, S. Dutcher, R. E. Kuehn, M. A. Vaughan, and B. Baum, 2008: Global Moderate Resolution Imaging Spectroradiometer (MODIS) cloud detection and height evaluation using CALIOP. *J. Geophys. Res.*, **113**, D00A19, doi:10.1029/2008JD009837.

Jensen, E. J., S. Kinne, and O. B. Toon, 1994: Tropical cirrus cloud radiative forcing: Sensitivity studies. *Geophys. Res. Lett.*, **21**, 2023–2026, doi:10.1029/94GL01358.

Jin, M., and S. Liang, 2006: An improved land surface emissivity parameter for land surface models using global remote sensing observations. *J. Climate*, **19**, 2867–2881, doi:10.1175/JCLI3720.1.

Jin, Z., T. P. Charlock, W. L. Smith Jr., and K. Rutledge, 2004: A parameterization of ocean surface albedo. *Geophys. Res. Lett.*, **31**, L22301, doi:10.1029/2004GL021180.

Khvorostyanov, V. I., and K. Sassen, 2002: Microphysical processes in cirrus and their impact on radiation. *Cirrus*, D. K. Lynch et al., Eds., Oxford University Press, 397–432.

Liou, K.-N., 1986: The influence of cirrus on weather and climate processes: A global perspective. *Mon. Wea. Rev.*, **114**, 1167–1199, doi:10.1175/1520-0493(1986)114<1167:IOCCOW>2.0.CO;2.

——, Q. Fu, and T. P. Ackerman, 1988: A simple formulation of the delta-four-stream approximation for radiative transfer parameterizations. *J. Atmos. Sci.*, **45**, 1940–1947, doi:10.1175/1520-0469(1988)045<1940:ASFOTD>2.0.CO;2.

——, Y. Gu, Q. Yue, and G. McFarguhar, 2008: On the correlation between ice water content and ice crystal size and its

application to radiative transfer and general circulation models. *Geophys. Res. Lett.*, **35**, L13805, doi:10.1029/2008GL033918.

Mace, G. G., Q. Zhang, M. Vaughan, R. Marchand, G. Stephens, C. Trepte, and D. Winker, 2009: A description of hydrometeor layer occurrence statistics derived from the first year of merged *CloudSat* and *CALIPSO* data. *J. Geophys. Res.*, **114**, D00A26, doi:10.1029/2007JD009755.

Min, M., P. Wang, J. R. Campbell, X. Zong, and Y. Li, 2010: Midlatitude cirrus cloud radiative forcing over China. *J. Geophys. Res.*, **115**, D20210, doi:10.1029/2010JD014161.

Protat, A., and Coauthors, 2014: Reconciling ground-based and space-based estimates of the frequency of occurrence and radiative effect of clouds around Darwin, Australia. *J. Appl. Meteor. Climatol.*, **53**, 456–478, doi:10.1175/JAMC-D-13-072.1.

Sassen, K., and B. S. Cho, 1992: Subvisual-thin cirrus lidar dataset for satellite verification and climatological research. *J. Appl. Meteor.*, **31**, 1275–1285, doi:10.1175/1520-0450(1992)031<1275:STCLDF>2.0.CO;2.

——, and J. R. Campbell, 2001: A midlatitude cirrus cloud climatology from the Facility for Atmospheric Remote Sensing. Part I: Macrophysical and synoptic properties. *J. Atmos. Sci.*, **58**, 481–496, doi:10.1175/1520-0469(2001)058<0481:AMCCCF>2.0.CO;2.

Stephens, G. L., and P. J. Webster, 1981: Clouds and climate: Sensitivity of simple systems. *J. Atmos. Sci.*, **38**, 235–247, doi:10.1175/1520-0469(1981)038<0235:CACSOS>2.0.CO;2.

——, S.-C. Tsay, P. W. Stackhouse Jr., and P. J. Flatau, 1990: The relevance of the microphysical and radiative properties of cirrus clouds to climate and climatic feedback. *J. Atmos. Sci.*, **47**, 1742–1753, doi:10.1175/1520-0469(1990)047<1742:TROTMA>2.0.CO;2.

——, and Coauthors, 2002: The *CloudSat* mission and the A-Train. *Bull. Amer. Meteor. Soc.*, **83**, 1771–1790, doi:10.1175/BAMS-83-12-1771.

Strahler, A. H., and Coauthors, 1999: MODIS BRDF/albedo product: Algorithm theoretical basis document version 5.0. NASA EOS-MODIS Doc. ATBD-MOD-09, 53 pp. [Available online at http://modis.gsfc.nasa.gov/data/atbd/atbd_mod09.pdf.]

Stubenrauch, C. J., and Coauthors, 2013: Assessment of global cloud datasets from satellites. *Bull. Amer. Meteor. Soc.*, **94**, 1031–1049, doi:10.1175/BAMS-D-12-00117.1.

Sun, W., G. Videen, S. Kato, B. Lin, C. Lukashin, and Y. Hu, 2011: A study of subvisual clouds and their radiation effect with a synergy of CERES, MODIS, *CALIPSO*, and AIRS data. *J. Geophys. Res.*, **116**, D22207, doi:10.1029/2010JG001573.

Thorsen, T. J., Q. Fu, and J. Comstock, 2011: Comparison of the *CALIPSO* satellite and ground-based observations of cirrus clouds at the ARM TWP sites. *J. Geophys. Res.*, **116**, D21203, doi:10.1029/2011JD015970.

Welton, E. J., J. R. Campbell, J. D. Spinhirne, and V. S. Scott, 2001: Global monitoring of clouds and aerosols using a network of micro-pulse lidar systems. *Lidar Remote Sensing for Industry and Environmental Monitoring*, U. N. Singh, T. Itabe, and N. Sugimoto, Eds., International Society for Optical Engineering (SPIE Proceedings, Vol. 4153), 151–158.

Winker, D. M., and Coauthors, 2010: The *CALIPSO* mission: A global 3D view of aerosols and clouds. *Bull. Amer. Meteor. Soc.*, **91**, 1211–1229, doi:10.1175/2010BAMS3009.1.

Yang, P., K. N. Liou, K. Wyser, and D. Mitchell, 2000: Parameterization of the scattering and absorption properties of individual ice crystals. *J. Geophys. Res.*, **105**, 4699–4718, doi:10.1029/1999JD900755.

——, H. Wei, H.-L. Huang, B. A. Baum, Y. X. Hu, G. W. Kattawar, M. I. Mischenko, and Q. Fu, 2005: Scattering and absorption property database for nonspherical ice particles in the near-through far-infrared spectral region. *Appl. Opt.*, **44**, 5512–5523, doi:10.1364/AO.44.005512.